A field trial to test the efficiency of induced partial saturation and horizontal drains to mitigate the susceptibility of soils to liquefaction

A. Flora, E. Bilotta, A. Chiaradonna, S. Lirer, L. Mele & L. Pingue

Bulletin of Earthquake Engineering
Official Publication of the European Association for Earthquake Engineering

ISSN 1570-761X

Bull Earthquake Eng
DOI 10.1007/s10518-020-00914-z

ONLINE FIRST

Springer

Your article is protected by copyright and all rights are held exclusively by Springer Nature B.V.. This e-offprint is for personal use only and shall not be self-archived in electronic repositories. If you wish to self-archive your article, please use the accepted manuscript version for posting on your own website. You may further deposit the accepted manuscript version in any repository, provided it is only made publicly available 12 months after official publication or later and provided acknowledgement is given to the original source of publication and a link is inserted to the published article on Springer's website. The link must be accompanied by the following text: "The final publication is available at link.springer.com”.

Springer

Author's personal copy

Bulletin of Earthquake Engineering
https://doi.org/10.1007/s10518-020-00914-z

S.I. : THE H2020 EUROPEAN PROJECT LIQUEFACT

A field trial to test the efficiency of induced partial saturation and horizontal drains to mitigate the susceptibility of soils to liquefaction

A. Flora[1] · E. Bilotta[1] · A. Chiaradonna[2] · S. Lirer[3] · L. Mele[1] · L. Pingue[4]

Received: 4 March 2020 / Accepted: 21 July 2020
© Springer Nature B.V. 2020

Abstract
Within the European project LIQUEFACT some activities have been devoted to the experimental verification of the effectiveness of two techniques in the mitigation of soil liquefaction susceptibility: induced partial saturation (IPS) and horizontal drains. After a preliminary check of their efficiency via centrifuge tests, the two techniques have been studied by means of some large scale shaking tests carried out in a field trial located in the Emilia-Romagna Region (Italy). A preliminary extensive in situ and laboratory investigation was necessary to identify the shallow liquefiable soil layer in which the mitigation techniques and the monitoring instrumentations (pore pressure transducers and geophones) had to be installed. Both techniques required the installation of horizontal well screens via a directional controlled drilling technique: the pipes were used as drainage systems (linear HDL and rhomboidal configurations HDR) or for the air injection in the area treated with IPS technique. The in situ experimental evidences showed that both techniques are able to avoid liquefaction triggering, that on the contrary was attained during the tests in the untreated testing area. The processing of in situ data highlighted that the efficiency of the two techniques is strictly related to chosen arrangement of the horizontal drains and the induced degree of saturation.

Keywords Soil liquefaction · Pilot test site · Laboratory tests · Horizontal drainage · Induced partial saturation

1 Introduction

Recent major earthquakes that hit many countries around the world (Christchurch 2010–2011; Emilia Romagna 2012; Palu 2018) have shown that the built environment is at risk not only because of inertial and kinematic forces directly induced on the structures by shaking, but also because of possible soil liquefaction phenomena. Earthquake induced soil liquefaction is a phenomenon marked by a rapid temporary reduction of soil shear strength and stiffness due to the build-up of pore water pressure which can occur in loose, saturated

✉ S. Lirer
s.lirer@unimarconi.it

Extended author information available on the last page of the article

Author's personal copy

Table 1 Classification of liquefaction mitigation techniques. Modified after Huang and Wen (2015)

Classification	Liquefaction mitigation method
Soil reinforcement	Soil replacement, addition of fines
	Soil densification: sand compaction pile, vibration compactions, dynamic compaction, blast compaction, compaction grouting
	Bonding of grains: permeation grouting, bio-cementation
Saturation degree reduction	Lowering of ground water table, Induced Partial Saturation
Drainage	Gravel piles, screen pipes

sandy deposits during the seismic shaking. During liquefaction, when the effective stresses approach zero, soil behavior switches from that of a solid to that of a fluid, causing serious damages to the build environment with loss of functionality and operative state of the constructed facilities.

The basic mechanisms ruling soil liquefaction phenomenon and the factors affecting liquefaction susceptibility have been deeply investigated in the last decades through cyclic undrained laboratory tests (Seed and Lee 1966; Silver et al. 1980; Ishihara 1985; Toki et al. 1986; Ishihara and Koseki 1989; Thevanayagam and Martin 2002; Mele et al. 2018; Mele et al. 2019c). Even though the earthquake induced liquefaction has been traditionally studied at laboratory scale, the ongoing experimental researches together with some new field evidences provided new insights regarding the in situ pore pressure generation within the soil, highlighted the relevance of some important aspects necessarily very simplified or neglected at the laboratory scale (Cubrinovski et al. 2018; Lirer et al. 2020), that can be analyzed only via large scale shaking tests (Rathje et al. 2004; Stokoe et al. 2014; Amoroso et al. 2020).

Many types of ground improvement techniques can be adopted to mitigate the liquefaction hazard in a cost-effective manner (Table 1): "direct" technologies, that act on the pore pressure changes causing liquefaction (e.g. drainage or desaturation), and "indirect" technologies, aimed to increase the soil capacity to resist at liquefaction attainment (soil reinforcement). Not all of them can be easily adopted in urban areas (i.e. blast compaction or dynamic compaction), where the mitigation intervention should avoid to disturb existing buildings and constructed facilities.

Within the Work Package 4 of the LIQUEFACT project, the team at the University of Napoli Federico II studied the effectiveness of some mitigation techniques: addition of fines (laponite), densification, induced partial saturation (IPS) and drainage systems.

The attention has been paid to the most suitable for the mitigation of the soil liquefaction hazard in densely urbanized areas:

- Horizontal Drains, HD;
- Induced Partial Saturation, IPS.

Generally speaking both techniques can be classified as "direct" technologies, but they work in two different ways: the horizontal drains accelerate the consolidation process within the soil, while the presence of (dispersed) air bubbles within the soil reduce the excess pore water pressure because of the very low volumetric stiffness of the gas phase.

The IPS technique has been studied by many researchers (Ishihara et al. 2002; Yegian et al. 2007; Okamura and Soga 2006; Mele et al. 2018) and it was recognized that even a

Author's personal copy

small reduction of the degree of saturation in soils initially completely saturated increase their resistance against liquefaction. Even though IPS is considered the most promising and innovative mitigation techniques, there are some uncertainness on which the research is ongoing, regarding its in situ application (injection of air/gas, use of bacteria) and its durability (Zeybek and Madabhushi 2017).

Within LIQUEFACT project, the Induced Partial Saturation and Horizontal Drains have been tested in physical models in the geotechnical centrifuge of ISMGEO s.r.l. (Seriate, Italy) and in a testing site that has been created on purpose by Trevi S.p.A. in a trial field located in the Emilia-Romagna Region (Pieve di Cento, Italy).

The paper describes in detail the large scales shaking tests performed in the field trial and the relative experimental results. The processing of the experimental data carried out in the test site highlighted the complexity of the liquefaction phenomenon in a real scale and the necessity to interpret the experimental results considering all the factors that affect the in situ soil response (dynamic loading source, partial drainage during shaking, layout of the treatment).

2 Test site

The test site is located in the Pieve di Cento municipality (Fig. 1, Emilia Romagna Region, Italy), a site that experienced widespread liquefaction manifestations after the mainshock of the 2012 seismic sequence ($M_L = 5.9$ and $M_L = 5.8$ on May 20 and 29 respectively). An extensive in situ investigation was preliminary carried out, aiming to define the ground layering and mechanical behaviour of the soils. Ground investigation was integrated with careful laboratory testing (monotonic and cyclic triaxial tests, oedometer tests, cyclic simple shear and cyclic torsional shear tests) on both disturbed and undisturbed specimens. The latter were retrieved by means of Gel-Pusher and Osterberg samplers.

In-situ investigation was carried out in the area where trial tests were planned, as shown in Fig. 2. In the Fig. 2a the traces of the pipes installed to act as horizontal drains (HD) or to insufflate air (IPS) are shown with continuous lines. Five boreholes were drilled, reaching 10 m depth (CH1bis, CH2, CH3, CH4, CH5), and four additional boreholes (CH2bis, CH3bis, CH4bis, CH5bis) were drilled to retrieve undisturbed samples. Electrical Resistivity Tomography (ERT) was also performed from the ground surface along the transept

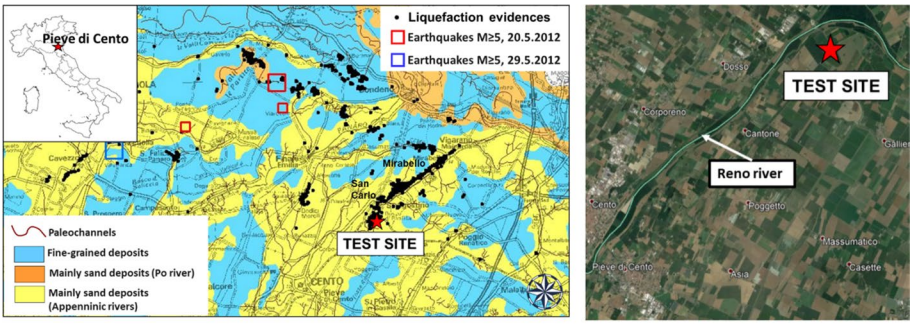

(a) (b)

Fig. 1 Location of the test site **a** with in black liquefaction evidences after 2012 Emilia EQ (Martelli and Romani 2013); **b** proximity to the Reno river

Author's personal copy

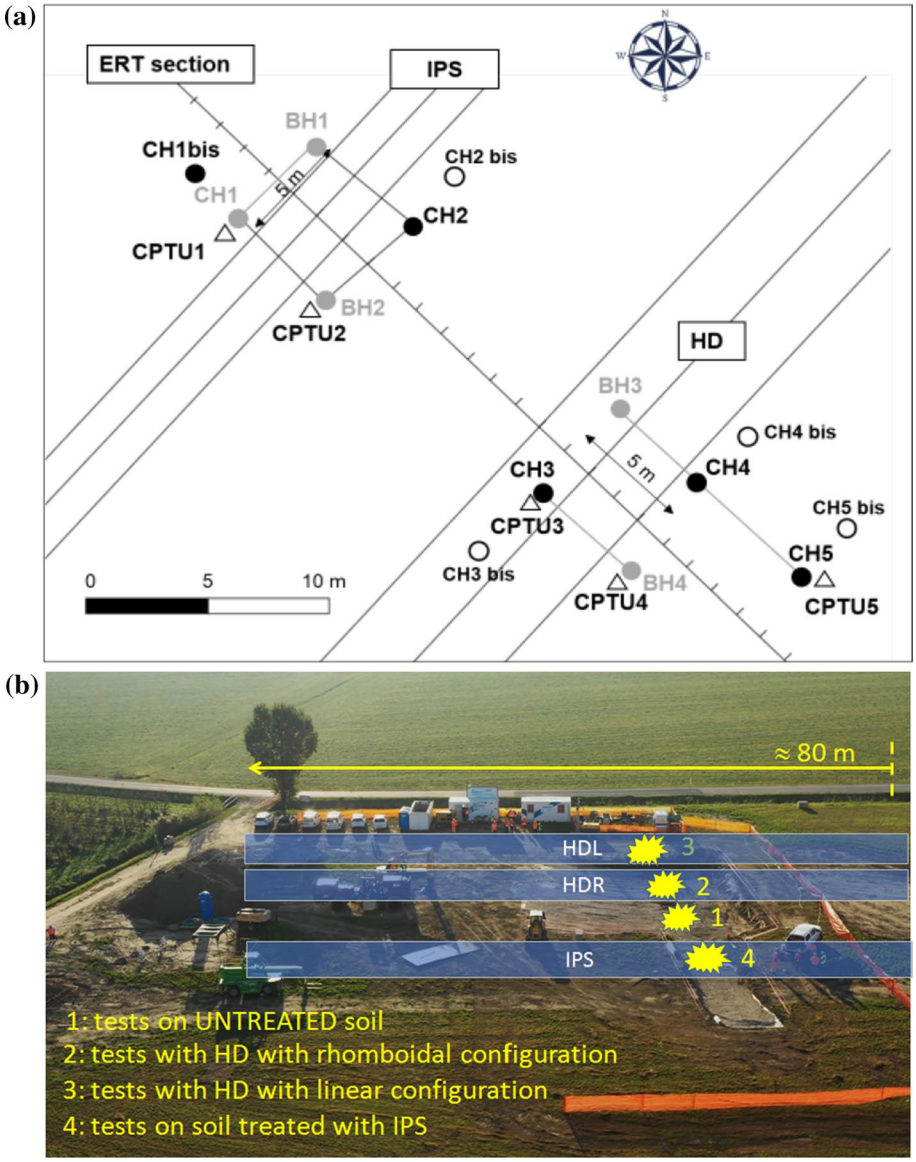

Fig. 2 Planview of the geotechnical in situ investigation (**a**) and aerial view of the test site (**b**)

shown in Fig. 2a. The ERT section was 71.25 m long and consisted of 96 electrodes located with a spacing of 0.75 m. Moreover, five penetration tests with piezocone (CPT_U) were carried out up to a depth of 11 m. Probing boreholes (BH1, CH1, BH2, BH3, BH4) were used for inserting vertical sensors in order to perform cross-holes tomography up to 10 m depth: cross-hole tomography was executed along four different alignments (i.e. BH1-CH1-BH2, BH1-CH2-BH2, BH3-CH4-CH5 and CH3-BH4), while a standard cross-hole test was performed between CH1-BH1 (Fig. 2a). Seismic cross-hole and cross-hole tomography

Author's personal copy

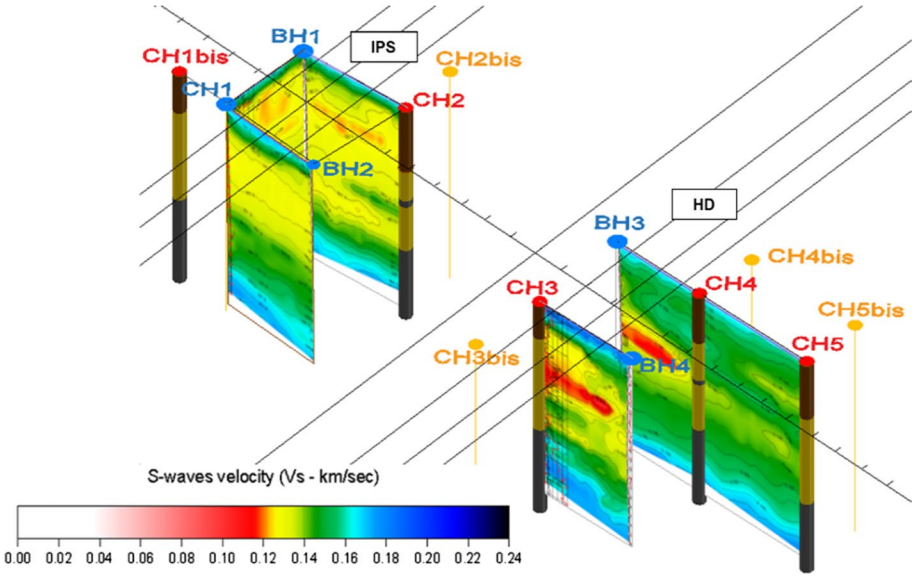

Fig. 3 Isometric view of the investigated site including the V_S distribution obtained by cross-hole tomographic survey

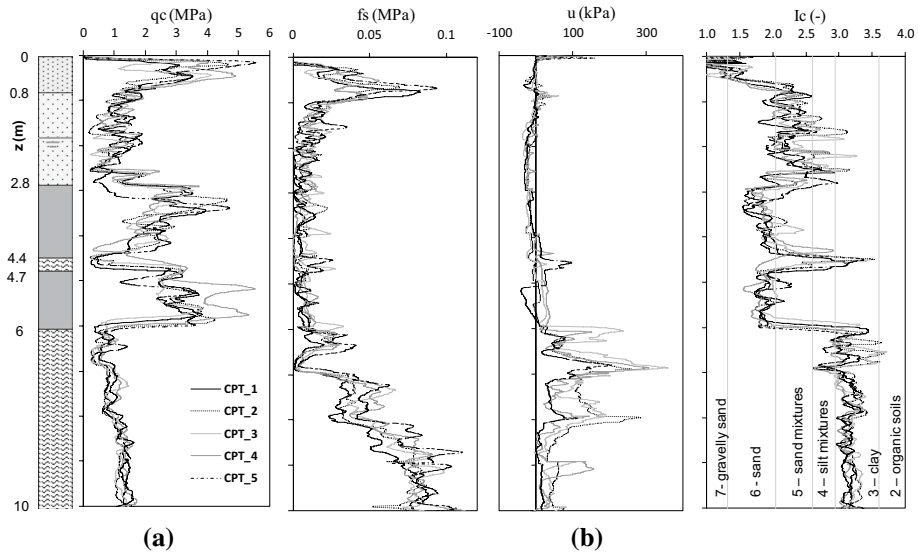

Fig. 4 CPTU tests results (**a**) and soil behaviour type Index Ic (**b**)

(Fig. 3) were carried out by using as receivers 3D sensors for measuring compression and shear wave velocities, V_P and V_S (Fig. 4), while as seismic source a sparker and an electrodynamic probe were used for generating compression and shear wave impulses, respectiv ely.

Author's personal copy

The depth of the ground water table is located at about 1.8 m below the ground level, as revealed by a piezometer installed at the time of the ground investigations (September 2017) and confirmed at the time of the liquefaction tests (October 2018).

Figure 4a shows the vertical profile of the cone tip resistance, q_c, the lateral resistance, f_s, and the measured pressure, u. The five profiles are quite homogeneous and greatly contributed to the identification of the soil stratigraphy. The thickness of the soil layers varies in the different boreholes even though the layering is more or less the same (Fig. 3), confirming the complexity of the geological background of the area (Martelli and Romani 2013; Paolucci et al. 2015). Despite such variability, from a practical point of view, the representative soil column consists (Table 2) of an upper crust of silty sand (SS) about 1.0 m thick and a sandy silt layer until approximately 2.8 m depth (BSS) overlying a grey silty sand deposit (GSS) between 2.8 and 6 m. A clayey formation (SC) is identified beyond 6 m depth from the ground surface. A thin layer of the same clay formation is identified in the middle of silty sand deposit, generally between 4.4 and 4.7 m depth, even though this is no clearly detectable in all the boreholes. Local reduction of V_S, corresponding to the thin clayey layer, are clearly detected in the sections returned from the cross-hole tomography (Fig. 3).

Figure 5 reports the V_S and V_P profiles returned by cross-hole tests: it is important to highlight that the thin clay layer interbedded in the grey silty sand (GSS) is not detected by the cross-hole tests, since the measured arrival times likely conform to those of the reflected head waves.

The CPT_U test results have been processed (Fig. 6) to identify the ground layering and some mechanical properties of the main formations, as the relative density D_r, (Kulhawy and Mayne 1990) and the shear strength angle φ‘ (Robertson and Campanella 1983) of the sandy layers ($0 < z < 6$ m). Soil behaviour type index I_c (Robertson 2009) has been also obtained (Fig. 4), thus identifying the liquefiable soil layers ($I_c < 2.6$).

The result of the ERT are reported in Fig. 7 in terms of distribution of soil resistivity (ρ) in the ground. In the same figure, the results of the CPT_U tests in terms of cone tip resistance q_c have been plotted, confirming the correlation with the ground layering identified by the ERT results.

Table 2 summarizes the average values of the soil mechanical properties obtained from the field survey.

Table 2 Representative soil column: soil properties obtained from the in situ test data

Depth (m)	Layer	Soil	Thickness (m)	V_S (m/s)	D_r (%)	φ_{pk} (°)	c′ (kPa)
0–1.0	SS	Silty sand	1	–	–	35	–
1.0–1.8	BSS	Brown silty sand	0.8	126	30	34	–
1.8–2.8	BSS	Brown silty sand	1	126	30	34	–
2.8–4.4	GSS1	Grey silty sand	1.6	130	38	35	–
4.4–4.7	SC1	Silty clay	0.3	117	–	27.5	15
4.7–6.0	GSS2	Grey silty sand	1.3	138	38	35	–
> 6.0	SC2	Silty clay	1	145	–	27.5	15
			1	154	–		
			1	163	–		

Author's personal copy

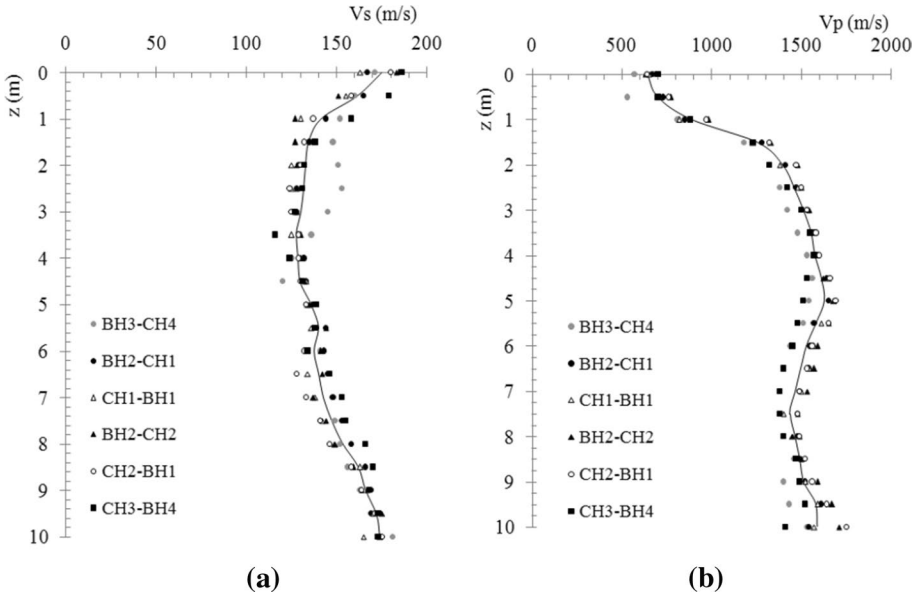

Fig. 5 Cross-hole results in terms of V_S (**a**) and V_P (**b**) profile

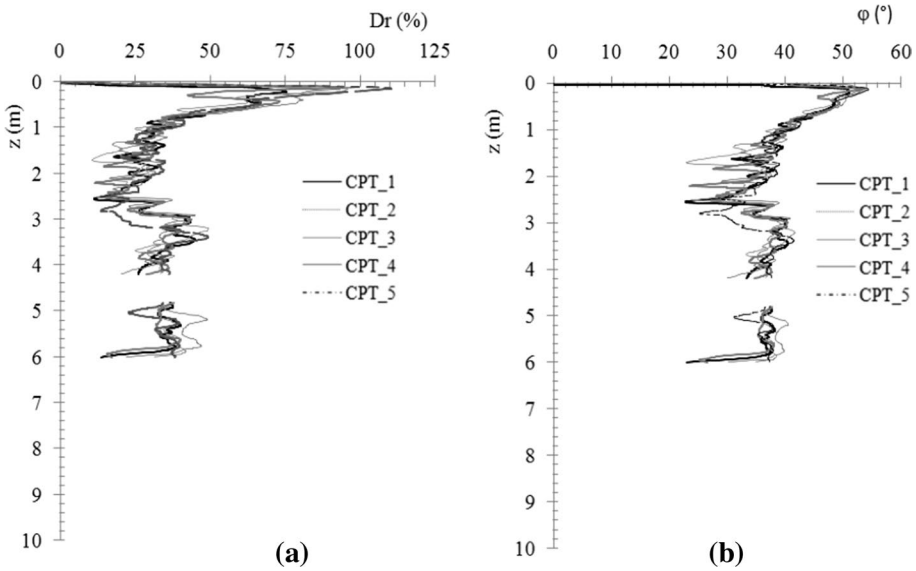

Fig. 6 Interpretation of CPTU tests in terms of soil relative density Dr (**a**) and shear strength angles profiles (**b**)

Author's personal copy

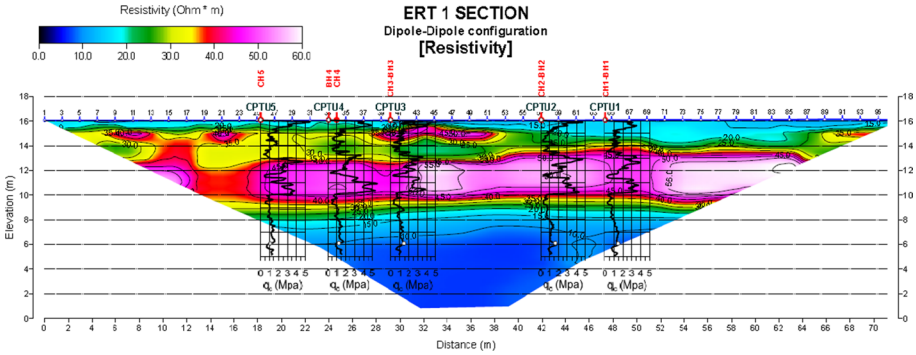

Fig. 7 ERT results in terms of resistivity contours and CPTu results

2.1 Laboratory testing

As previously mentioned, the in situ investigation was integrated with laboratory tests: to this aim, undisturbed samples (by means of Gel-Pusher and Osterberg samplers) have been retrieved in the sandy deposit located under the ground water level (Fig. 8). Additionally, some reconstituted specimens of the shallow sandy layers have been tested, that were obtained from the soil retrieved by a backhoe in the first 2 meters. Soils grading and physical properties are shown respectively in Fig. 9 and Table 3.

The shallower layer of silty sand ($1 < z < 2.8$ m) is characterized by a brownish colour, hence named Brown Silty Sand (BSS), while the deeper sand ($2.8 < z < 6.0$) has a greyish colour and it has been named Grey Silty Sand (GSS). The shallower layer BSS is constituted by heterogeneous soils (well-graded and with variable fine content and low-plasticity fine), while the underlying GSS is quite homogeneous, with a fine content ranging from 5–12%. The clayey layer SC ($4.4 < z < 4.7$ m and $z > 6$ m) has a plasticity index $I_p = 0.55$ and can be assumed as impervious.

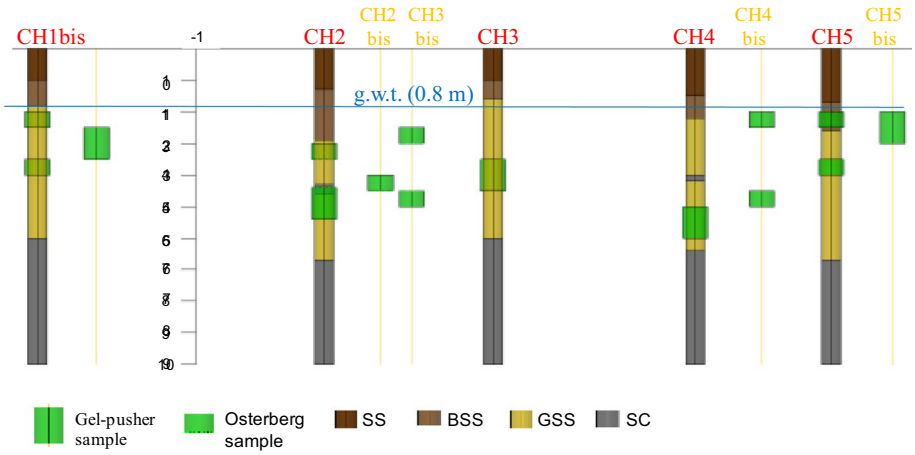

Fig. 8 Representative soil profile with location of soil sampling

Author's personal copy

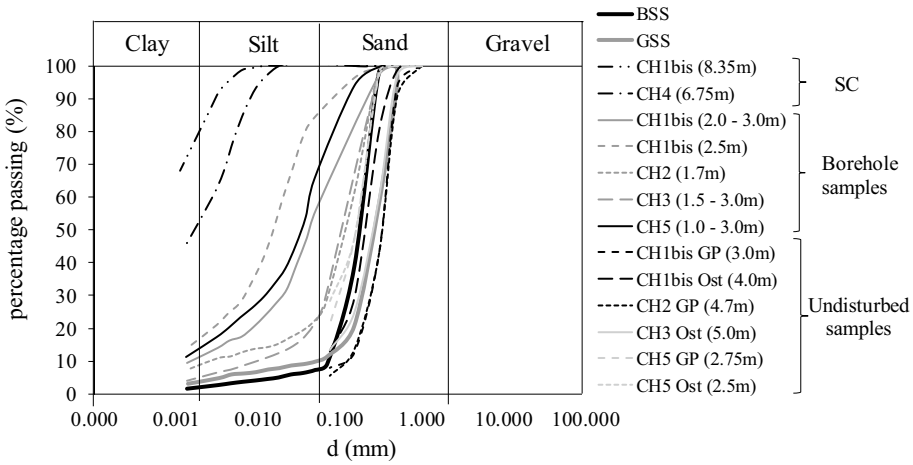

Fig. 9 Grain size distribution of tested soils

Table 3 Properties of Pieve di Cento soils

Soil	G_s	e_{max}–e_{min}	D_{50} (mm)	FC (%) (d < 0.075 mm)	I_p	k (m/s)[a]
BSS	2.667	1.04–0.546	0.18	8	–	1.0×10^{-4}
GSS	2.655	0.884–0.442	0.30	12	–	1.8×10^{-5}
SC	2.699	–	–	–	0.55	–

[a]Estimated by means of laboratory permeability tests

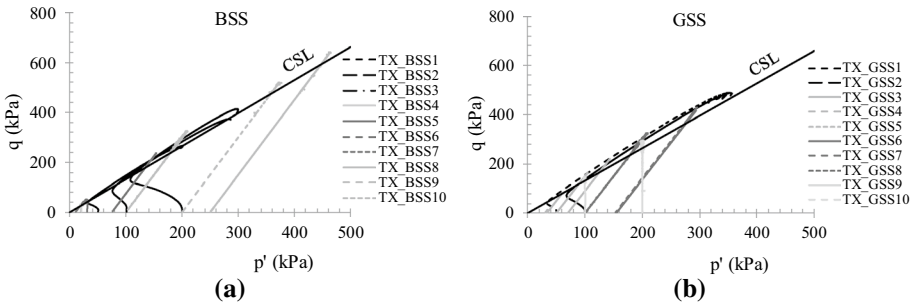

Fig. 10 Results of monotonic triaxial tests on reconstituted specimens of GSS (**a**) and BSS (**b**) in the deviatoric plane q–p′ (details in "Appendix")

The mechanical behavior of BSS and GSS has been investigated by means of triaxial TX and simple shear SS tests carried out, under monotonic and cyclic loading conditions, on soil specimens reconstituted by wet pluviation at the same in situ relative density (Fig. 6a) and on undisturbed specimens (Mele et al. 2019a, b). Such tests have been summarized in "Appendix".

Author's personal copy

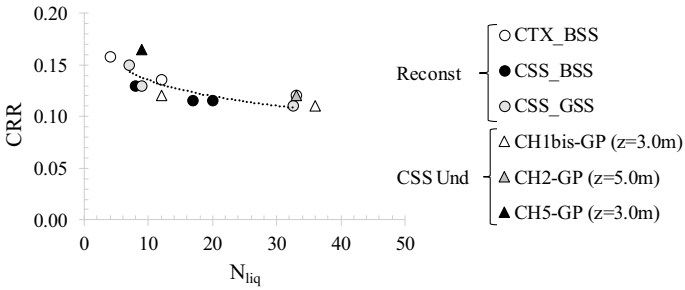

Fig. 11 Results of cyclic tests (triaxial CTX and simple shear tests CSS) on reconstituted and undisturbed specimens of BSS and GSS soils (average relative density Dr ≈ 45%, details in "Appendix")

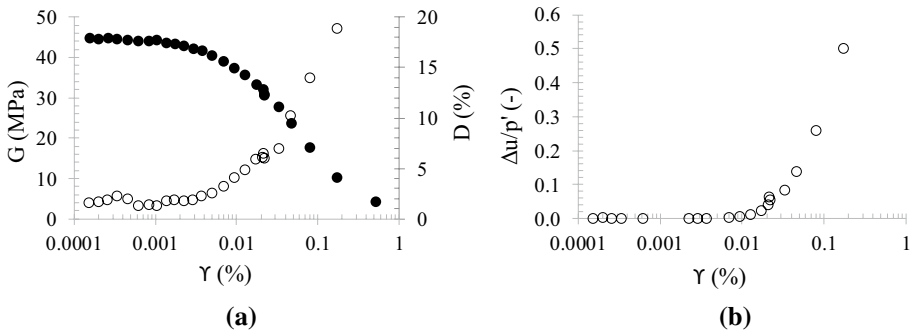

Fig. 12 Results of torsional shear test on undisturbed specimen BSS (confining stress σ′ = 60 kPa)

The results of the monotonic drained and undrained triaxial tests (Table 5) are plotted in Fig. 10 in the deviatoric plane q–p′ (where q is the deviatoric stress and p′ the mean effective stress).

The results of the monotonic tests highlighted that BSS and GSS reach the same value of the stress ratio M ($q/p' = M_{cs} = 1.32$) at the critical state, corresponding to an average value of the shear strength friction angle ($\varphi'_{ave} \approx 33°$), that is consistent with the values obtained by the processing of the in situ CPT_U tests (Fig. 6b).

As previously mentioned, some undrained cyclic tests have been carried out to quantify the soil resistance to earthquake induced liquefaction (expressed by the Cyclic Resistance Ratio, CRR).

In Fig. 11, the results of the cyclic tests (CTX and CSS) have been represented via the well-known cyclic resistance curve $CRR - N_{liq}$. The liquefaction triggering (N_{liq}) has been experimentally identified in terms of induced excess pore water pressure Δu by means of the well known pore pressure ratio r_u ($r_u = \Delta_u/\sigma'_v = 0.9$).

It is worth noting that the results of cyclic triaxial tests (CTX, Table 6), to be represented together with those of cyclic simple shear tests (CSS, Tables 7, 8), have been corrected through Castro's correlation (Castro 1975), assuming a coefficient k_0 (σ'_h/σ'_v) equal to 0.48, congruently with the value measured performing cyclic simple shear tests by means of flexible boundary (Mele et al. 2019c).

Author's personal copy

It can be noted again that a unique cyclic resistance curve CRR-N_{liq} is identified for both soils GSS and BSS: the results confirm also that the technique of preparation of the reconstituted specimens did not affect the cyclic response of a geological young soil.

Additionally, a torsional shear test (Table 9) has been carried out on an undisturbed specimen of GSS (CH3; z = 4.0 m; e_0 = 0.778). The results of the test are plotted in Fig. 12 in the typical planes γ–G–D and γ–G/G_0–r_u, where γ is the shear strain, G is the shear modulus and D is damping ratio. The value of G_0 is equal to 45 MPa (Fig. 12), consistent with the V_s in situ measurement at the same confining stress and density conditions.

2.2 Liquefaction potential assessment for Pieve di Cento site

The main shock of the Emilia 2012 earthquake sequence occurred on May 20, 2012 at 02:03:53 UTC time. Liquefaction manifestations, i.e., sand boils and longitudinal cracks, were observed at the Pieve di Cento site after the event (Fig. 13). The collected CPT_U data have been used to evaluate liquefaction triggering for the 2012 earthquake using a state-of-the-practice simplified analysis procedure (Boulanger and Idriss 2016), assuming level ground and free-field conditions.

As for previous numerical studies pertaining to the same area (Sinatra and Foti 2015; Chiaradonna et al. 2019), aground motion prediction equation (GMPE) based on the Italian strong-motion database has been adopted for estimating the expected value of PGA at the site (Bindi et al. 2011).

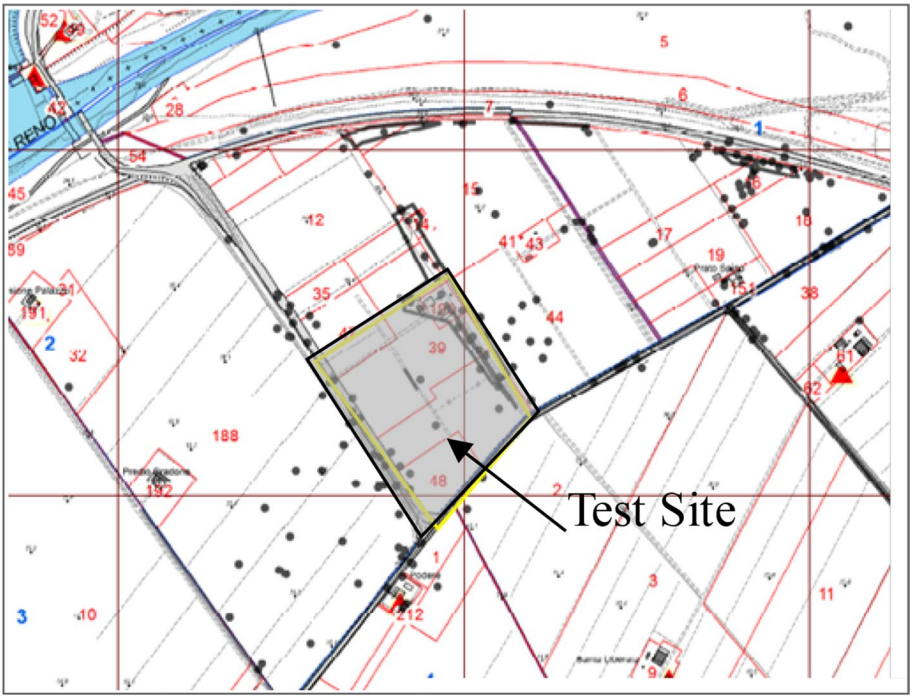

Fig. 13 Map of liquefaction evidences (black point) after the 20.05.2012 earthquake

Author's personal copy

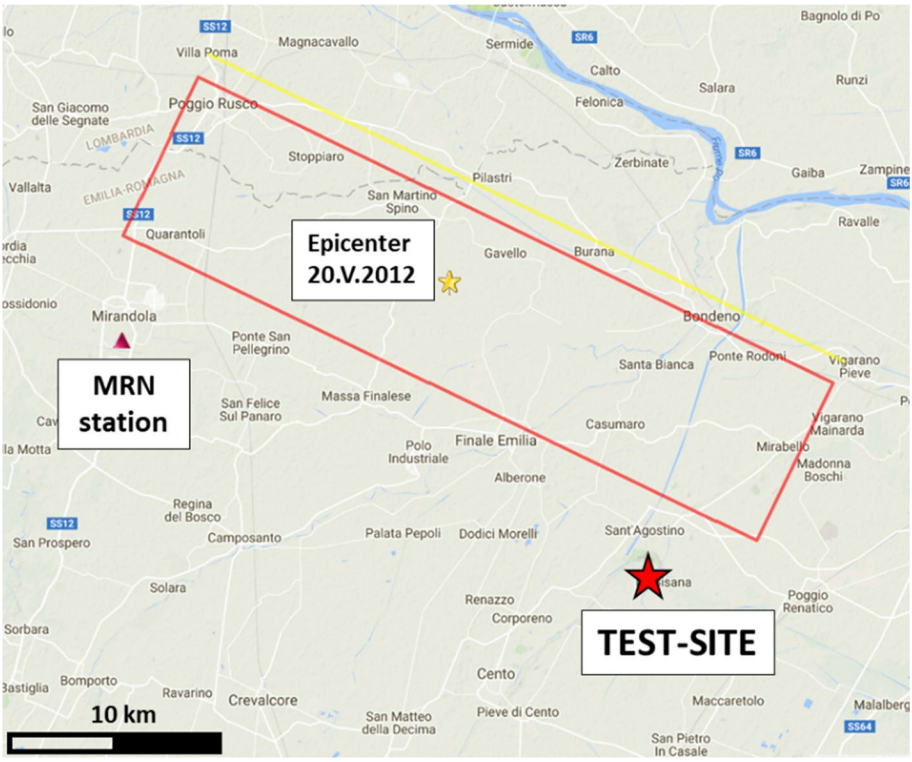

Fig. 14 Fault projection on the ground surface and epicentre of the 20.05.2012 earthquake with location of the MRN station and test-site

The MRN station of the Italian strong-motion network (RAN), located in Mirandola town, is the closest to the epicentre (Fig. 14) and recorded a peak ground acceleration, PGA, as high as 0.27 g. Since the Pieve di Cento test-site and MRN station have the same Joyner-Boore, R_{JB}, distance and they have the same site conditions (Class C site according to Eurocode 8),according to the adopted attenuation law the expected PGA is the same at the both sites.

Liquefaction triggering was evaluated using the Boulanger and Idriss (2016) CPT-based procedure, which compares at different depths (z) the earthquake-induced cyclic stress ratio CSR (computed via the well-known Seed and Idriss procedure 1971) to the cyclic resistance ratio CRR of the soil to estimate the factor of safety against liquefaction (FS = CRR/CSR).

Figure 15 reports the results of the simplified liquefaction evaluation procedure as vertical profiles of the CSR, CRR and the safety factor FS, confirming that the seismic demand CSR of the 2012 Emilia earthquake is well above the soil capacity CRR (FS < 1).

Moreover, in order to take into account the uncertainties in the assessment of the seismic motion, the cyclic stress ratio CSR has been evaluated also by means of dynamic analyses in total stress, according to an equivalent linear approach (code STRATA, Kottke et al. 2013). A set of 7 recorded acceleration time histories have been selected to be compatible with the elastic acceleration response spectrum prescribed by the Italian Building code

Author's personal copy

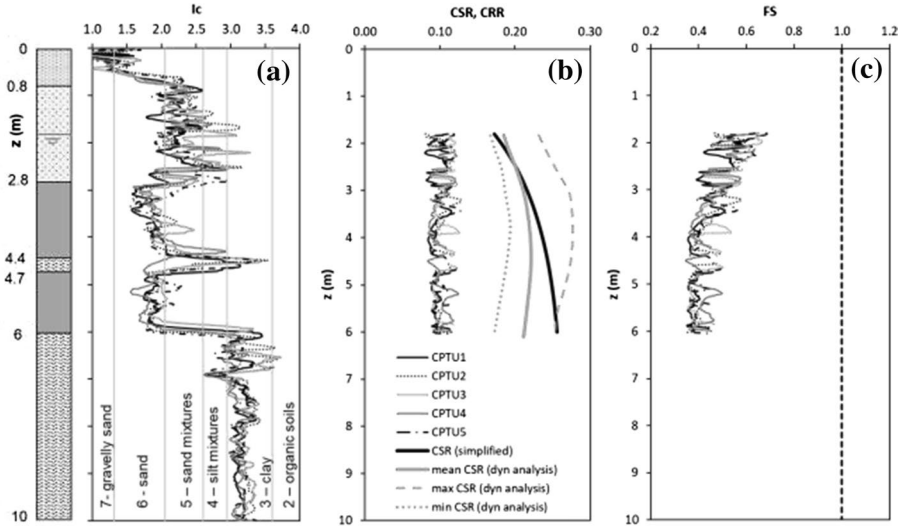

Fig. 15 Assessment of liquefaction potential for Pieve di Cento test site: profile of Ic (**a**); CRR defined on CPTu results, CSR obtained from the stress-based simplified method and min, max and mean range of CSR obtained form dynamic analyses (**b**) and safety factor FS against liquefaction calculated according to the simplified method (**c**)

NTC2018 at the considered site for a return period of 475 years. Further constrains adopted in the selection of the records and the details of the analyses are reported in Chiaradonna et al. (2020), here not repeated for sake of brevity.

Figure 15b shows that the CSR obtained from the simplified method is included in the range of variability of CSR predicted by the dynamic analyses. The simplified method leads to the most conservative scenario (if compared to the mean CSR profile of the dynamic analyses) and it has been adopted in the computation of the safety factor against liquefaction FS (Fig. 15c).

3 Testing areas

In the aerial view of the Pieve di Cento site (Fig. 2), four testing areas can be identified:

- Untreated area 1 (UN).
- Treated area 2: horizontal drains with a rhomboidal configuration (HDR).
- Treated area 3: horizontal drains with a linear configuration (HDL).
- Treated area 4: induced partial saturation (IPS).

The mitigation interventions (HDL, HDR and IPS) and the relevant monitoring instrumentation (Fig. 16) have been located in the upper part of the GSS layer ($2.8 < z < 4.4$ m). As previously mentioned, this is the liquefiable layer nearest to the ground surface, were the dynamic loading source (a shaker, later described and shown in Fig. 17, Table 4) has been located, with the aim of producing a significant pore pressure build-up, possibly triggering soil liquefaction.

Author's personal copy

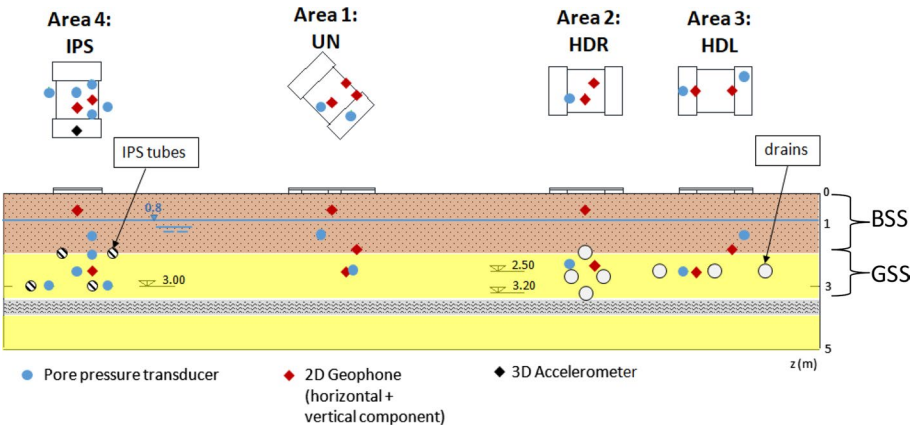

Fig. 16 Field test configurations: cross section of the four testing areas

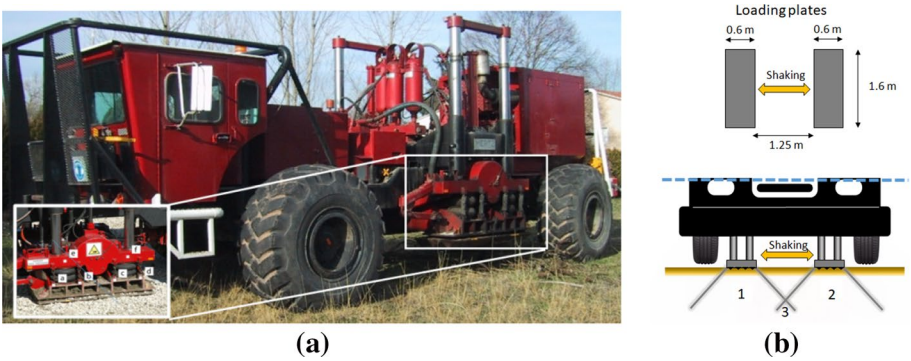

Fig. 17 Adopted shaker (**a**) and scheme of the loading plates (**b**)

Table 4 Main features of the adopted shaker

Type	M13S/609 S-WAVE
Maker	MertzInc
Hold down weight	178 kN
Reaction mass	3175 kg
Base plate	0.6 × 1.6 m
Peak force	138 kN
Frequency range	3–80 Hz

In each area, some pore pressure transducers and bi-directional geophones have been deployed in order to measure the pore pressure increments (Δu) and the vertical and the horizontal (in the direction of the applied shaking) components of velocity. The position of the shaker in all the shaking tests has been changed in order to guarantee that the direction of the applied shaking was aligned with the geophones installed in the subsoil.Before

Author's personal copy

testing, a preliminary 1 m deep excavation was realized in all the areas in order to locate the shaker as closer as possible to the liquefiable GSS layer.

The adopted shaker (M13S/609 S-Wave, Fig. 17 and Table 4) has two base plates (A_{bp} = 0.6 m × 1.6 m) with a saw tooth surface to ensure a good coupling with the base soil. It is evident that the soil volume beneath the two loading plates is potentially influenced by the presence of initial shear stresses (boundary of zone 1, 2 and 3 in Fig. 17b). The vibrator imposes in-plane cyclic movements of the base plates and generates pure shear waves into the subsoil only if the machine is perfectly horizontal and keeps this position during the tests. In the case of an irregular settlement of the machine, some tilting occurs and therefore the motion applied at ground level also generated a vertical cyclic component of action.

In each test, the static vertical self weight of the shaker was first applied and, after waiting for consolidation process by monitoring excess pore water pressure dissipation within the underneath soil, a dynamic loading was applied for a duration ranging between 100 s and 200 s (Fig. 18). During all the shaking tests, the settlements of the base plates of the shaker have been measured via topographic measurements.

Twelve tests have been performed: five in the untreated area, four in the areas with drainage systems and three in the area were induced partial saturation has been applied. Some tests have been interrupted for problems occurred during shaking (e.g. large tilting of the machine) or for a malfunctioning of some of the installed monitoring instruments. In the paper, only the tests fully monitored will be described in detail.

3.1 Untreated area 1

The untreated area 1 (Fig. 16) has been instrumented with two pore pressure transducers (Fig. 19). Concerning the measurement of the ground shaking, three geophones have been deployed into the ground to measure soil velocity: a shallow one (G-VS-1) in the BSS layer above the water level, and the other two (G-VS-2 and G-VS-3) deeper in the GSS layer.

3.2 Well screen and their installation technique for treated areas

In all the treated areas, innovative well screens were set in place: they are made of micropored polyethylene and have been designed to minimize flow resistance by means of a

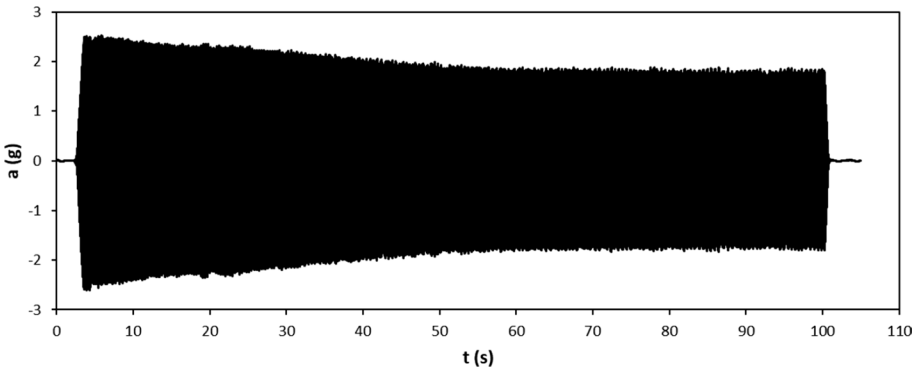

Fig. 18 Recorded horizontal acceleration on the base plate of the shaker (for a test at f = 10 Hz)

Author's personal copy

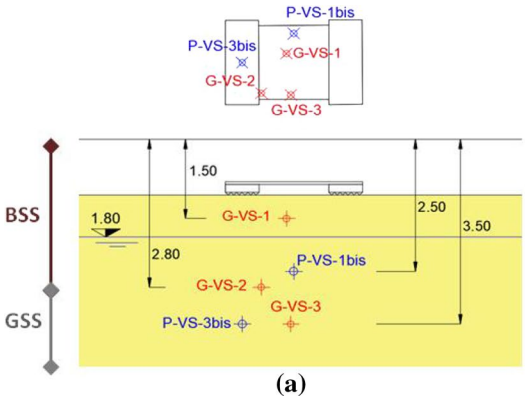

(a)

Instruments	Name	z (m)
Pore pressure transducer	P-VS-1bis	1.5
	P-VS-3bis	2.5
Geophone	G-VS-1	0.5
	G-VS-2	1.8
	G-VS-3	2.5

(b)

Fig. 19 Geometrical scheme of the cross sections of the untreated area 1

greater porosity—compared to conventional ones—uniformly distributed along the pipe's entire length. It has been also possible to choose within a wide range of pore size in order to match the well screens characteristics to both: soil formation and geotechnical application. The pipes were installed by means of the Directional Drilling Technique DDT that actually represents a whole set of techniques changing according to the type of soil/rock. It allows to be always in control during drilling where being in control means, first of all, to be able to know, at any time, the actual position of the drilling bit then, if necessary, to be able to modify the drilling path at will. This technology was derived from oil industry, where it is mostly used to achieve high verticality in extremely long drillings, and it is now commonly used to achieve a very high accuracy through steered path.

The applied drilling technique and installation sequence, described in next sections, allowed to target the following challenges:

- Installing each element according to a very well defined horizontal and vertical spacing;
- Avoiding/minimizing settlements during installation;
- Minimizing ground disturbance before shaking.

The installation methodology and sequence represent a solution which can be easily adopted also below existing structures (Fig. 20).

DDT application for LIQUEFACT test field used an electric cable deployed on the ground, as an artificial magnetic field source. A special probe equipped with tri-axial accelerometers and magnetometers, temperature sensors and digitizing circuitry was used for real-time survey of the drilling path, and slant bit (Fig. 21) was used for steering in the sandy soils to be drilled through.

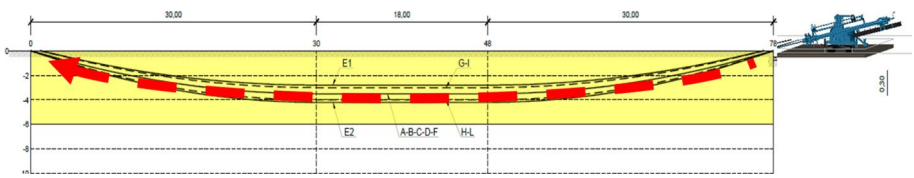

Fig. 20 Layout of DDT application at the site

Author's personal copy

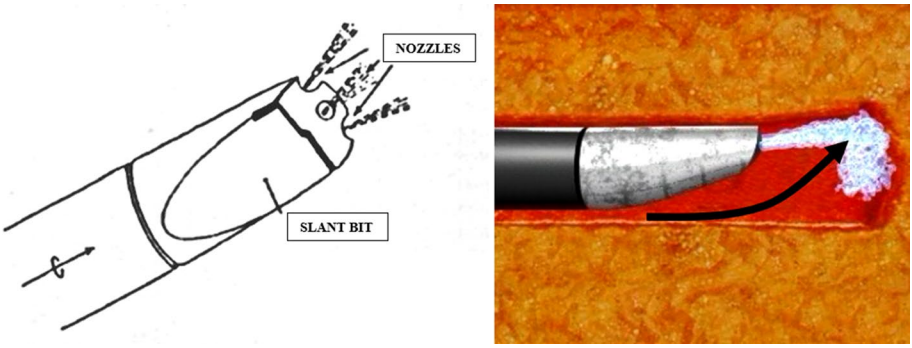

Fig. 21 Slant bit for directional drilling used at LiqueFACT test field

Fig. 22 Drilling equipment set-upduring directional drilling activities

The presence on site of the Steering Engineer and the driller, continuously in communication each other by walkie-talkie, together with the use of a very light solution of 100% biodegradable polymer solution allowed to achieve a real challenging goal: all pipes were successfully installed at the ground level and with a final average deviation from the theoretical path of 13 cm in the middle section (Fig. 22), it worth also to mention that no significant settlements at ground level were noted.

3.3 Treated areas 2 and 3: horizontal drains (HDL and HDR)

For the Horizontal Drains, OD/ID (mm) 180/150 Grade SO80 well screens with an internal reinforcement mesh were installed. Such a large diameter was necessary to increase the draining surface while the reinforcement minimized the risk of pipes damage during installation.

The final goal was to set in place seven high porosity polyethylene micro-pored horizontal well screens according to two different geometrical configurations (Fig. 23):

- A linear configuration HD-L: three draining pipes (A, B, C with a spacing of about 1.8 m located at the depth of 3.5 m from the original ground level, Fig. 23a);
- A rhomboidal configuration HD-R: four draining pipes (E1, E2, D, F with a spacing of about 1.0 m located at the depths of 2.8 m, 3.5 m and 4.2 m from the original ground level, Fig. 23a).

Author's personal copy

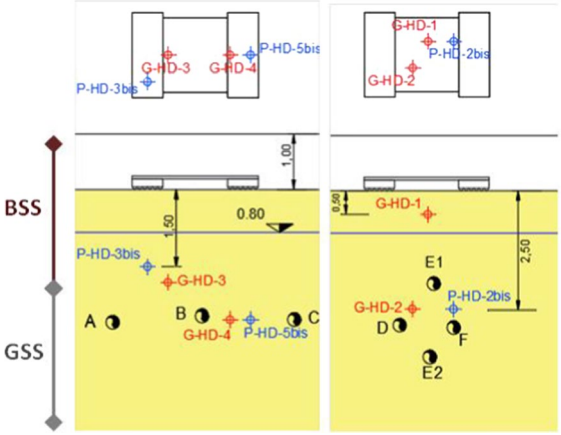

(a) (b)

Instruments HD-L (a)	Name	z (m)
Pore pressure transducer	P-HD-3bis	1.50
	P-HD-5bis	2.50
Geophone	G-HD-3	1.80
	G-HD-4	2.50

Instruments HD-R (b)	Name	z (m)
Pore pressure transducer	P-HD-2bis	2.50
Geophone	G-HD-1	0.50
	G-HD-2	2.50

(c)

Fig. 23 Geometrical scheme of the cross sections of the treated areas 2 and 3 (HD-L and HD-R)

The cross section on the areas 2 and 3 is reported in Fig. 23a, with the depth (Fig. 23b) of all the installed instruments referred to the new ground surface were the vibrating source was located.

Pipes installation required a bowed drilling path having a total length of about 78 m divided into three stretches. The first curved stretch (~30 m) starting from ground level with a radius of curvature ranging roughly between 100 and 120 m to reach the required depth; the second horizontal stretch (~18 m) and the third curved stretch (~30 m) heading upwards to the ground surface, with a radius of curvature ranging roughly between 100 and 120 m.

In order to reduce soil disturbance to a minimum, the following installation sequence was adopted. During drilling with DDT technology Ø76 mm steel rods, the rod chain was connected to a Ø200 mm reamer with swivel device; then withdrawn by reaming the hole through 100% biodegradable polymer slurry to guarantee stability. Meantime the 78 m head-to-head welded pipes were assembled on site: 30 m of HDPE blind pipes, followed by 18 m Grade SO80 patented screen pipes and, again, 30 m of blind pipes. The reamer was connected

Fig. 24 Final withdrawal of HD well screens, starting point (left) final point (right)

Author's personal copy

to a steel wire inserted into the 78 m head-to-head welded pipes, allowing to be withdrawn by reaming the hole and installing the screen pipes (Fig. 24). Reamers with a diameter exceeding by just 10% the pipes' diameter and a low viscosity natural biodegradable polymer slurry, as drilling fluid, have been used to reduce soil disturbance during the installation.

3.4 Treated areas 4: induced partial saturation (IPS)

The partial saturation of the soil below the ground water table was obtained by injecting pressurized air from four sub horizontal well screens deployed in two rows at the depths of 3.0 and 4.0 m (G, I, H, L in Fig. 25) from the original ground level, with a horizontal spacing of 2 m. For the IPS, OD/ID (mm) 75/60 Grade SO40 well screens without internal reinforcement mesh were installed (grade 040 is the porosity recommended for the air-injection as typical application). The use of double packers to dissect the section of pipe to inject air through, made it necessary not to resort to internal reinforcement for IPS pipes. That is because a perfect adherence between the blown-up packer and pipe was required.

The installation of the IPS pipes was very similar to that of HD pipes, although it was rather simpler due to the significantly lower lateral friction of pipes, hence significant lower risk of breakage during withdrawing. Since the diameter of IPS pipes was lower than for the HD pipes, a smaller reamer (Ø90 mm) was adopted in this case (Fig. 26).

In this area (Fig. 25a) five pore pressure transducers and two geophones were placed into the ground at different depths (z) from the vibrating source (Fig. 25b).

A rough assessment of the ground volume to be treated allowed to quantify the amount of air volume to be injected into the soil, taking into account a certain percentage of injected air lost through the boreholes. It has been quantified (Flora et al. 2019) that the injection of about 15 m^3 of air should be well suited to obtain a final value of S_r higher than 80%, a value low enough to guarantee a significant increase of the cyclic resistance of the treated GSS soil volume (Mele et al. 2018). The air was pumped into the pipes at a pressure high enough to

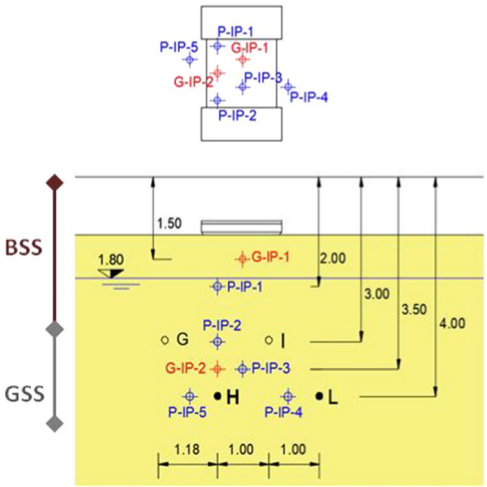

(a)

Instruments IPS	Name	z (m)
Pore pressure transducer	P-IP-1	1.0
	P-IP-2	2.0
	P-IP-3	2.5
	P-IP-4	3.0
	P-IP-5	3.0
Geophone	G-IP-1	0.5
	G-IP-2	2.5

(b)

Fig. 25 Geometrical scheme of the cross sections of the treated area 4 (IPS)

Author's personal copy

Fig. 26 Adopted reamer for HD (left) and IPS (right)

overcome the water hydrostatic pressure, but not so high to generate soil displacement or erosion (p = 30 kPa for the shallowest pipes and 40 kPa for the deepest alignment).

Some preliminary insufflations tests have been carried to verify the IPS procedure and to check the induced degree of saturation S_r in the treated soil volume. To this aim, Cross-Hole and ERT in situ tests were carried out, respectively measuring the velocity of compression waves V_P and the soil resistivity ρ, both sensitive to a change in the saturation degree. Some uncertainness remain on the most effective way to in situ measure the degree of saturation: the processing of the V_p data is affected by the correct interpretation of the traveling distance of the P-waves (the fastest P-waves may not be those travelling on the shortest length because the head P-waves at the saturated–unsaturated interface were faster than those travelling in the unsaturated soil), while the ERT tests present less criticalities, but they are less common and less sensitive to small variations in the range of extremely high degrees of saturation. The processing of both data obtained after the preliminary insufflations tests highlights that for this specific case, the results of ERT tests have been much more reliable than the V_p measurements (Flora et al. 2019).

4 In situ shaking tests

4.1 Results in the untreated area 1

The results of the test UN_2 performed on the natural soil has been considered as reference datasets. In this test a shaking long enough to induce measurable effects within the soils was adopted (time of shaking 100 s + 100 s). The data recorded by the geophones (Fig. 27) showed that the motion applied by the shaker was transmitted into the soil: the large values of the components of velocity (horizontal and vertical) have been registered by the upper geophone (G-VS-1, Fig. 27), and a sharp reduction was registered in the velocities recorded by the deeper ones (G-VS-2 and G-VS-3). As expected, a vertical cyclic component of action has been also recorded in all the geophones, following the irregular settlements of the machine.

The shaking applied at the ground surface induced the build-up of pore water pressure within the soil (Fig. 28). The highest values of the excess pore water pressure Δu (Fig. 28a) was recorded, as obvious, by the shallower pressure transducer P-VS-1bis (z = 1.5 m), that is closer to the vibrating source. The liquefaction triggering was checked via the pore pressure ratio r_u computed by taking into account the self-weight of the shaker in the

Author's personal copy

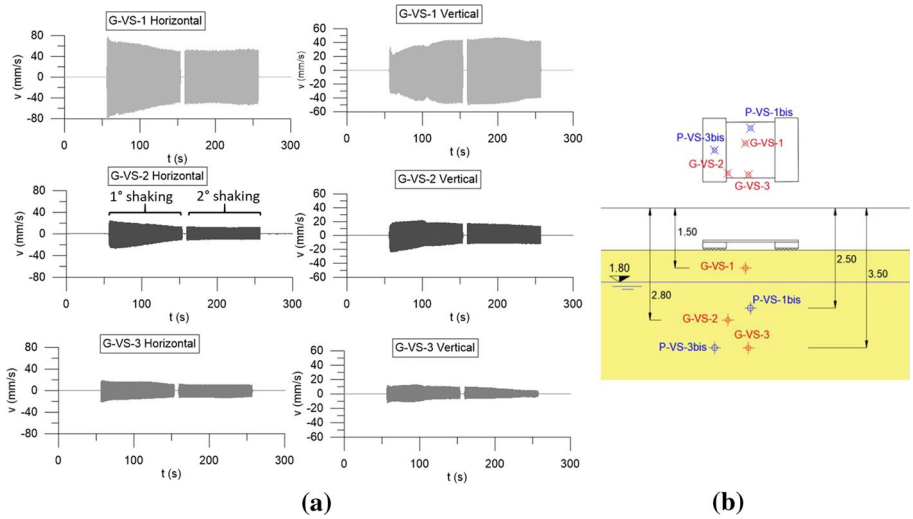

Fig. 27 Results of test UN_2 in the area 1: time histories of the horizontal and vertical components of velocity (**a**) measured by the geophones placed into the soil, and geometrical scheme of the cross sections of the area 1 (**b**)

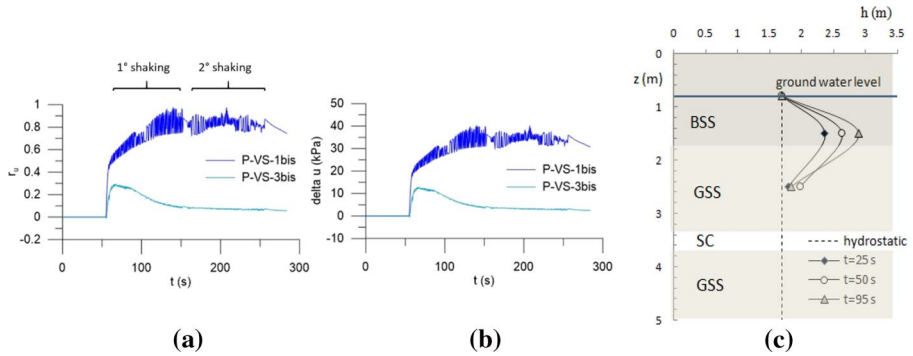

Fig. 28 Results of test UN_2 in the area 1: (**a**) excess pore water pressure Δu and (**b**) pore pressure ratio r_u; (**c**) hydraulic head profiles at three different instants of time t from the start of shaking

computation of the effective vertical stress σ'_v. To be as close as possible to the actual 3D increase of the vertical effective stress, the σ'_v values at the exact location of the sensors have been computed by means of a 3D numerical model of the site performed with the finite difference code FLAC 3D (v.6, Itasca 2016). In the model the overall weight of the S-vibrator has been applied to the area of the two base plates (Fig. 17b) and an elastic perfectly plastic soil model obeying the Mohr–Coulomb failure criterion has been adopted for all the soil layers, according to the properties reported in Table 2.

It can be noted that at the shallow depth (z = 1.5 m) the dynamic input triggered the soil liquefaction ($r_{u,max} = 0.9$) after 80 s of shaking. The deeper pore water transducer P-VS-3bis (z = 2.5 m) measured lower values of excess pore water pressure ($r_{u,max} = 0.3$) according to the lower dynamic action recorded by the geophone at this depth (G-VS-2, Fig. 27).

Author's personal copy

(a) (b)

Fig. 29 Test UN_2 in the area 1: (**a**) picture of sand ejecta during the test and (**b**) shaker loading plate upon retrieval at the end of the test

The time histories r_u-t reveal that after a relatively short fully undrained phase of shaking, the measured pore pressure increments were certainly affected by a partial drainage (Fig. 28b).

The development of a complex water flow during the shaking is proven by the hydraulic head (h) profiles, plotted in Fig. 28c for three different times after the start of the shaking (t = 25, 50 and 95 s): it can be noted that during shaking vertical water flow patterns develop both upwards and downwards.

After liquefaction triggering, sand ejecta was observed (Fig. 29a) immediately around the shaking plates. The shaking continued for other 100 s, but it did not affect the excess pore water pressure measured within the soil. During this second part of the test, very large settlements of the loading plate were measured with a continuously increasing tilting of the shaker. The average final vertical displacement of the vibrating plates was in this test 32 cm, which brought the pistons loading the shaking plates to reach their full span before the programmed end of the test (Fig. 29b).

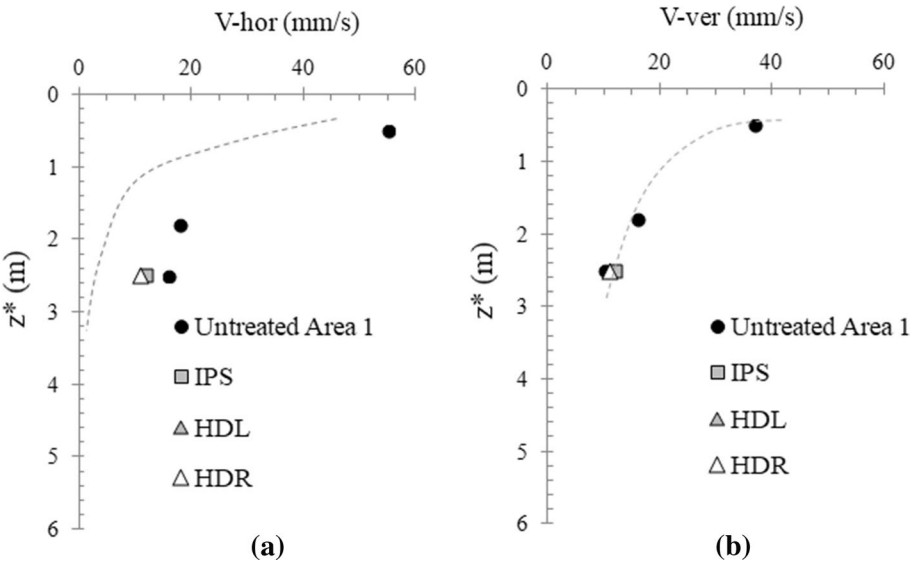

Fig. 30 Comparison among the average values of the horizontal (**a**) and vertical (**b**) components of the soil velocity measured by the geophones in all the testing areas (z* = depth from the excavated new ground surface)

Author's personal copy

4.2 Results in the treated areas

The shaking tests have been repeated in the areas (area 2, 3 and 4) in which the mitigation technique had been implemented, in order to verify if and how the soil response is affected by the chosen mitigation techniques. As previously described, the horizontal drains were installed in two different configurations (HDL and HDR) in order to analyze the effect of different layouts on the effectiveness of the technique. Concerning the IPS technique, the tests in the area 4 have been carried out after the injection of about 15 m^3 of air, the amount of air volume necessaryto obtain a final value of $S_r > 80\%$.

The shaking tests in all the tested areas have been performed using the same dynamic signal adopted in the untreated area 1 (Fig. 18): as expected, the motion measured by the geophones becomes weaker with depth (Fig. 30). In all the tests, a vertical component of the velocity has been measured, confirming that the shaker systematically underwent rocking during all the tests. The comparison in terms of soil motion among all the four different tests can be done at the depth z = 2.5 m, where there was a working geophone in all the testing areas: the results plotted in Fig. 30 demonstrate that, for the same input given at the ground level, the same type of shaking has been transmitted into the ground.

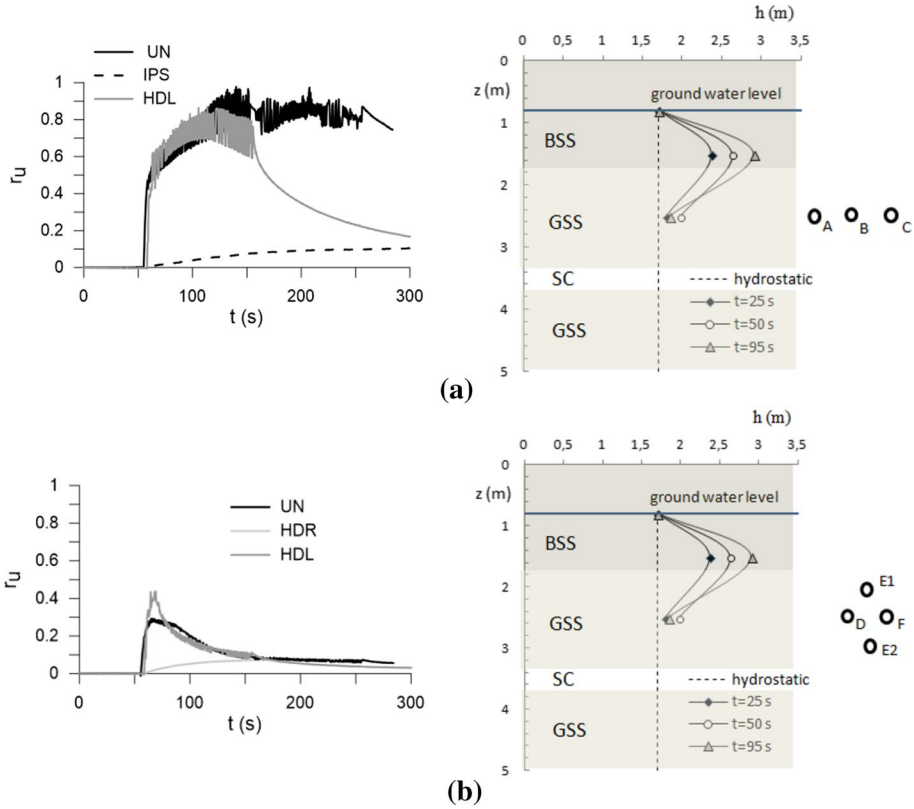

Fig. 31 Comparison among pore pressure ratio time histories computed in the testing areas at (**a**) 1–1.5 m and (**b**) 2.5 m depth from the ground surface

Author's personal copy

The shaking tests are compared in Fig. 31 in terms of pore pressure ratio time histories (related to the first 100 s of shaking) computed at two different depth from the dynamic source, were the pore pressure transducers have been placed.

The pore pressure ratio time histories of r_u experienced at the shallow depth ($1.0 < z < 1.5$ m) in three of four areas are shown in Fig. 31a: the results in the area conditioned with drains deployed in a linear layout (HDL) and in that subjected to Induced Partial Saturation (IPS), are compared with those obtained in the untreated area 1. Data from the rhomboidal layout of drains (HDR) are missing since at this depth no pressure transducer was installed.

It can be noted (Fig. 31) that the drains in the linear configuration have a very low effectiveness, since only a slightly lower value of the peak excess pore pressure ratio is achieved compared to that measured in the untreated area ($r_{u,max,HDL} \approx 0.8$ *vs* $r_{u,max} \approx 0.9$), thanks to a faster rate of excess pore pressure dissipation. On the contrary, the IPS technique is very effective in reducing the excess pore water pressure, giving a value of $r_{u,max,IPS} \approx 0.1$.

The comparison among the experimental data pertaining to all the tested area is possible at the deeper depth $z = 2.5$ m (Fig. 31b): the results confirm again that the linear configuration of the horizontal drains (HDL) is not able to mitigate the pore pressure buildup. On the contrary, drains deployed in the rhomboidal layout are very effective in reducing the pore pressure build up, achieving a peak value of $r_{u,max,HDR} \approx 0.1$. Consistently with the results obtained at the shallow depth, the IPS technique is again the most effective one, giving the lower values of the induced excess pore water pressure ($r_{u,max,IPS} \approx 0.05$).

The field results pertaining to the drains deployed in the linear configuration reveal the inability of such configuration to act on the drainage process within the soil. A possible reason of these results can be connected to the chosen depth of the draining line (Fig. 31a): by looking at the vertical water flow pattern developed in the untreated area, that can be inferred from Fig. 28c, the drains should have been located at a shallower position (i.e. $z = 1.5$ m), where the maximum value of the excess pore water pressure were expected (higher values of the hydraulic head). This is probably the reason why the rhomboidal configuration, that includes also one drain (E1, Fig. 31b) in a shallower position, was more effective in the pore pressure dissipation.

In the treated areas no fluid sand ejecta and no water outcome have been observed, confirming that no full liquefaction has been attained in these areas. The average final vertical displacement of the vibrating plates was of about 15 cm in the areas 2 (HDR) and 3 (HDL) and less than 10 cm in the area treated with IPS technique.

5 Concluding remarks

The Induced Partial Saturation and Horizontal Drains have been deeply studied in the European Project LIQUEFACT as sustainable techniques for the mitigation of soil liquefaction susceptibility in urbanised areas.

The effectiveness of both techniques was studied by means of some large scale shaking tests carried out in a field trial located in Emilia Romagna Region (Italy), where different testing areas have been instrumented with pore pressure transducers and geophones to monitor the ground response to a dynamic action applied at the ground surface by a shaking machine.

Both techniques required the installation of innovative micropored polyethylene well screens (used as drainage system or to inject air) via a Directional Drilling Technique that guarantees to install pipes horizontally in the liquefiable soil layer, at a specified depth from the ground surface.

Author's personal copy

The experimental evidences obtained from the field trial tests showed that both techniques are able to avoid liquefaction triggering, that on the contrary was attained during the tests in the untreated testing area. The large amount of data registered during the tests constitutes a valuable dataset to have an insight into the complex mechanism of liquefaction, partial drainage, and effect of de-saturation.

Even though the tests can be considered successful, there are unavoidable uncertainties in the interpretation of tests results, mostly because of the chosen geometrical set up of horizontal drains and also on the true degree of saturation induced by IPS. In particular, the horizontal drains (HDR) were efficient in the pore pressure dissipation when deployed in a rhomboidal layout, achieving a value of r_u comparable to the one obtained with the IPS treatment. On the contrary, the linear layout (HDL) was not so effective because of the depth chosen for the pipes, that were too deep to increase the rate of the dissipation of the Δu.

Induced partial saturation was extremely effective ($r_{u,max,IPS.} \approx 0.1$), thus confirming to be a promising means to tackle liquefaction risk in densely urbanized areas.

Appendix

See Tables 5, 6, 7, 8 and 9.

Table 5 Results of monotonic triaxial tests on Pieve di Cento (BSS and GSS) sands

Test	Sand	σ'_c (kPa)	Stress path	e_0^a	D_{r0}^a (%)	e_{cs}	p'_{cs} (kPa)
TX_BSS1	PdC_BSS	50	C_CIU	0.765	55.7	0.705	201.1
TX_BSS2	PdC_BSS	100	C_CIU	0.784	51.8	0.784	286.0
TX_BSS3	PdC_BSS	200	C_CIU	0.773	54.0	0.773	302.1
TX_BSS4	PdC_BSS	20	C_CID(p′)	0.830	42.5	0.858	20.0
TX_BSS5	PdC_BSS	30	C_CID(p′)	0.712	66.4	0.746	30.0
TX_BSS6	PdC_BSS	10	C_CID	0.795	49.6	0.825	21.1
TX_BSS7	PdC_BSS	75	C_CID	0.863	35.8	0.875	143.0
TX_BSS8	PdC_BSS	100	C_CID	0.761	56.5	0.779	183.1
TX_BSS9	PdC_BSS	200	C_CID	0.719	65.0	0.714	357.9
TX_BSS10	PdC_BSS	250	C_CID	0.784	51.8	0.780	412.4
TX_GSS1	PdC_GSS	50	C_CIU	0.658	51.1	0.658	364.2
TX_GSS2	PdC_GSS	100	C_CIU	0.649	53.2	0.649	360.7
TX_GSS3	PdC_GSS	30	C_CID	0.656	51.6	0.687	54.3
TX_GSS4	PdC_GSS	50	C_CID	0.622	59.3	0.646	92.2
TX_GSS5	PdC_GSS	70	C_CID	0.684	45.2	0.706	132.1
TX_GSS6	PdC_GSS	100	C_CID	0.720	37.1	0.721	189.2
TX_GSS7	PdC_GSS	150	C_CID	0.695	42.8	0.701	273.2
TX_GSS8	PdC_GSS	150	C_CID	0.730	34.8	0.739	277.7
TX_GSS9	PdC_GSS	100	C_CID(p′)	0.650	52.9	0.695	100.0
TX_GSS10	PdC_GSS	200	C_CID(p′)	0.726	35.7	0.743	200.0

CID consolidate isotropically drained, *CIU* consolidate isotropically undrained, *CID(p′)* consolidate isotropically drained with p′ constant, *C* compression, *E* extension

[a]At the end of consolidation phase

Author's personal copy

Table 6 Results of cyclic triaxial tests on BSS sand (Mele et al. 2019a)

Test	Sand	σ'_c (kPa)	e_0^a	D_{r0}^a (%)	CSR	N_{liq} $r_u = 0.90$	N_{liq} $\varepsilon_{DA} = 5\%$
CTX_BSS1	PdC_BSS	50	0.808	47.0	0.210	4.0	4.6
CTX_BSS2	PdC_BSS	56	0.828	42.9	0.160	33.0	> 34
CTX_BSS3	PdC_BSS	50	0.769	54.9	0.180	12.0	14.0

[a]At the end of consolidation phase

Table 7 Cyclic simple shear tests on reconstituted loose and dense sandy soils (Mele et al. 2019b)

Test	Sand	Prep. Tech	σ'_h (kPa)	σ'_v (kPa)	e_0^a	D_{r0}^a (%)	CSR	N_{liq} (r_u)	N_{liq} (γ)
CSS_BSS1F	BSS	1D-C	33.4	58.9	0.818	44.9	0.130	8	6
CSS_BSS2F	BSS	1D-C	23.8	61.5	0.834	41.7	0.115	17	17
CSS_BSS3F	BSS	1D-C	29.3	60.5	0.805	47.6	0.115	20	19
CSS_BSS4F	BSS	1D-C	44.8	60.0	0.659	77.1	0.155	3.5	1.5
CSS_BSS5F	BSS	1D-C	28.9	59.5	0.653	78.3	0.135	23	20
CSS_BSS6F	BSS	1D-C	34.5	60.6	0.656	77.7	0.160	13	13
CSS_GSS1F	GSS	1D-C	42.8	80.1	0.634	56.6	0.150	7	5
CSS_GSS2F	GSS	1D-C	27.2	58.6	0.683	45.5	0.130	9	8.5
CSS_GSS3F	GSS	1D-C	27.0	54.7	0.713	38.7	0.113	33	35
CSS_GSS8F	GSS	1D-C	24.0	49.0	0.581	68.6	0.150	11	9
CSS_GSS9F	GSS	1D-C	24.8	43.9	0.598	64.7	0.130	> 70	70
CSS_GSS10F	GSS	1D-C	25.2	49.7	0.574	70.1	0.165	10	9

[a]At the end of consolidation phase

Author's personal copy

Table 8 Results of cyclic simple shear tests on undisturbed specimens of Pieve di Cento sand

Test	Borehole	Sampler	Depth (m)	e_0	σ'_h (kPa)	σ'_v (kPa)	e_c^a	CSR	N_{liq} (r_u)	N_{liq} (γ)
CSS_CH1_O1	CH1bis	Ost	3.6	0.680	23.6	76.1	0.653	0.100	320	260
CSS_CH1_O2	CH1bis	Ost	3.8	0.622	19.6	51.3	0.613	0.130	24	> 26
CSS_CH1_O3	CH1bis	Ost	4.0	0.603	19.2	51.2	0.593	0.140	26	> 28
CSS_CH1_O4	CH1bis	Ost	4.0	0.682	20.0	51.0	0.675	0.140	68.6	> 70
CSS_CH5_GP1	CH5	GP	3.0	0.654	12.7	44.3	0.648	0.095	No	No
CSS_CH5_GP2	CH5	GP	3.0	0.714	13.8	32.8	0.692	0.165	9	7
CSS_CH5_O1	CH5	Ost	2.5	0.949	11.9	28.5	0.908	0.170	175	180
CSS_CH5_O2	CH5	Ost	2.0	0.877	20.5	41.1	0.855	0.150	188	> 190
CSS_CH2_GP1	CH2	GP	5.0	0.668	23.3	60.4	0.655	0.120	33	34
CSS_CH1_GP1	CH1bis	GP	3.0	0.697	13.6	40.5	0.692	0.110	36	> 40
CSS_CH1_GP2	CH1bis	GP	3.1	0.631	13.9	41.4	0.623	0.120	12	> 12
CSS_CH3_O1	CH3	Ost	4.8	0.546	24.1	61.0	0.533	0.120	> 80	> 80
CSS_CH3_O2	CH3	Ost	5.0	0.658	24.2	61.8	0.650	0.140	53	> 53

[a] At the end of consolidation phase

Author's personal copy

Table 9 Torsional shear tests on undisturbed specimen of Pieve di Cento sand (Flora et al. 2019)

Test	Material	Undisturbed sampler	Depth (m)	e_0
TS_CH3_GP	Sandy soil	Gel Pusher CH3	4.00	0.778

References

Amoroso S, Rollins KM, Andersen P, Gottardi G, Tonni L, Martínez MFG, Wissmann K, Minarelli L, Comina C, Fontana D, Monaco P, Pesci A, Sapia V, Vassallo M, Anzidei M, Carpena A, Cinti F, Civico R, Coco I, Conforti D, Doumaz F, Giannattanasio F, Di Giulio G, Foti S, Loddo F, Lugli S, Manuel RM, Marchetti D, Mariotti M, Materni V, Metcalfe B, Milana G, Pantosti D, Pesce A, Salocchi AC, Smedile A, Stefani M, Tarabusi G, Teza G (2020) Blast-induced liquefaction in silty sands for full-scale testing of ground improvement methods: insights from a multidisciplinary study. Eng Geol 265:105437

Bindi D et al (2011) Ground motion prediction equations derived from the Italian strong motion database. Bull Earthq Eng 9(6):1899–1920

Boulanger RW, Idriss IM (2016) CPT-based liquefaction triggering procedure. J Geotech Geoenviron Eng 142(2):04015065

Castro G (1975) Liquefaction and cyclic mobility of saturated sands. J Geotech Environ Eng 101:551–569

Chiaradonna A, Tropeano G, d'Onofrio A, Silvestri F (2019) Interpreting the deformation phenomena of a levee damaged during the 2012 Emilia earthquake. Soil Dyn Earthq Eng 124:389–398. https://doi.org/10.1016/j.soildyn.2018.04.039

Chiaradonna A, Lirer S, Flora A (2020) A liquefaction potential integral index based on pore pressure build-up. Eng Geol. https://doi.org/10.1016/j.enggeo.2020.105620

Cubrinovski M, Rhodes A, De la Torre C, Bray J, Ntritsos N (2018) Liquefaction hazards from "inherited vulnerabilities". In: XVI Danube, European conference on geotechnical engineering, June 2018, Skopje, R. Macedonia

Flora A, Chiaradonna A, Bilotta E, Fasano G, Mele L, Lirer S, Pingue L, Fanti F (2019) Field tests to assess the effectiveness of the ground improvement for liquefaction mitigation. Invited lecture. In: Proceedings of the 7th international conference on earthquake geotechnical engineering, 7ICEGE, Rome (Italy), June 2019ISBN: 978-0-367-14328-2 (Hbk), eISBN: 978-0-429-03127-4 (eBook)

Huang Y, Wen Z (2015) Recent development of soil improvement method for seismic liquefaction mitigation. Nat Hazards 2015(76):1927–1938

Ishihara K (1985) Stability of natural deposits during earthquakes. In: Proceedings of the 11th international conference on soil mechanics and foundation engineering, vol 1, pp 321–376

Ishihara K, Koseki J (1989). Cyclic shear strength of fines-containing sands. In: Proceeding 12th international conference of soil mechanics, Rio de Janeiro, pp 101–106

Ishihara K, Tsukamoto Y, Nakazawa H, Kamada K, Huang Y (2002) Resistance of partly saturated sand to liquefaction with reference to longitudinal and shear wave velocities. Soils Found 42(6):93–105

Itasca (2016) FLAC 3D, fast Lagrangian analysis of continua, version 6.0 computer program and the user's guide, Itasca Consulting Group Inc

Kottke AR, Wang X, Rathje EM (2013). Technical manual for strata. Geotechnical Engineering Center, Department of Civil, Architectural and Environmental Engineering, University of Texas

Kulhawy FH, Mayne PW (1990) Manual on estimating soil properties for foundation design (no. EPRI-EL-6800). Electric Power Research Institute, Palo Alto, CA (USA); Cornell University, Ithaca, NY (USA). Geotechnical Engineering Group

Lirer S, Chiaradonna A, Mele L (2020) Soil liquefaction: from mechanisms to effects on the built environment. Rivista Italiana di Geotecnica 3/2020. https://doi.org/10.19199/2020.2.0557-1405.025

Martelli L, Romani M (2013) Microzonazione sismica e analisi della condizione limite per l'emergenza delle aree epicentrali dei terremoti della pianura emiliana di maggio-giugno 2012 (Ordinanza del commissario delegato n. 70/2012), Relazione Illustrativa. http://ambiente.regione.emilia-romagna.it **(in Italian)**

Mele L, Tan Tian J, Lirer S, Flora A, Koseki J (2018) Liquefaction resistance of unsaturated sands: experimental evidence and theoretical interpretation. Géotechnique. https://doi.org/10.1680/jgeot.18.p.042

Mele L, Lirer S, Flora A (2019a) The specific deviatoric energy to liquefaction in saturated cyclic triaxial tests. In: Proceedings of the 7th international conference on earthquake geotechnical engineering,

Author's personal copy

7ICEGE, Rome (Italy), June 2019 ISBN: 978-0-367-14328-2 (Hbk), eISBN: 978-0-429-03127-4 (eBook)

Mele L, Lirer S, Flora A (2019b) The effect of densification on Pieve di Cento sands in cyclic simple shear tests. In: National conference of the researchers of geotechnical engineering. Springer, Cham, pp 446–453

Mele L, Lirer S, Flora A (2019c) The effect of confinement in liquefaction tests carried out in a cyclic simple shear apparatus. In: Proceedings of the 7th international symposium on deformation characteristics of geomaterials, IS-Glasgow 2019, Glasgow (Scotland)

Okamura M, Soga Y (2006) Effects of pore fluid compressibility on liquefaction resistance of partially saturated sand. Soils Found 46(5):695–700

Paolucci E, Albarello D, D'Amico S, Lunidei E, Martelli L, Mucciarelli M, Pileggi D (2015) A large scale ambient vibration survey in the area damaged by May–June 2012 seismic sequence in Emilia Romagna, Italy. Bull Earthq Eng 13(11):3187–3206

Rathje EM, Chang WJ, Stokoe KH, Cox BR (2004) Evaluation of ground strain from in situ dynamic response. In: Proceeding of the 13th world conference on earthquake engineering

Robertson PK (2009) Interpretation of cone penetration tests—a unified approach. Can Geotech J 46(11):1337–1355

Robertson PK, Campanella RG (1983) Interpretation of cone penetration tests. Part I: Sand. Can Geotech J 20(4):718–733

Seed HB, Idriss IM (1971) simplified procedure for evaluating soil liquefaction potential. J Soil Mech Found Div ASCE 97(SM9):1249–1273

Seed HB, Lee KL (1966) Liquefaction of saturated sands during cyclic loading. J Soil Mech Found Div 92(6):105–134

Silver ML, Tatsuoka F, Phukunhaphan A, Avramidis AS (1980) Cyclic undrained strength of sand by triaxial test and simple shear test. In: Proceedings of the 7th world conference on earthquake engineering, pp 281–288

Sinatra L, Foti S (2015) The role of aftershocks in the liquefaction phenomena caused by the Emilia 2012 seismic sequence. Soil Dyn Earthq Eng 75:234–245

Stokoe KH, Roberts JN, Hwang S, Cox BR, Menq FY, Van Ballegooy S (2014) Effectiveness of inhibiting liquefaction triggering by shallow ground improvement methods: Initial field shaking trials with T-Rex at one site in Christchurch, New Zealand. In: Soil liquefaction during recent large-scale earthquakes, p 193

Thevanayagam S, Martin GR (2002) Liquefaction in silty soils—screening and remediation issues. Soil Dyn Earthq Eng 22:1035–1042

Toki S, Tatsuoka F, Miura S, Yoshimi Y, Yasuda S, Makihara Y (1986) Cyclic undrained triaxial strength of sand by a cooperative test program. Soils Found 26(3):117–128

Yegian MK, Eseller-Bayat E, Alshawabkeh A, Ali S (2007) Induced-partial saturation for liquefaction mitigation: experimental investigation. J Geotech Geoenviron Eng ASCE 133(4):372–380

Zeybek A, Madabhushi GSP (2017) Durability of partial saturation to counteract liquefaction. Proc Inst Civ Eng Ground Improv 170(2):102–111

Publisher's Note Springer Nature remains neutral with regard to jurisdictional claims in published maps and institutional affiliations.

Affiliations

A. Flora[1] · E. Bilotta[1] · A. Chiaradonna[2] · S. Lirer[3] · L. Mele[1] · L. Pingue[4]

A. Flora
flora@unina.it

E. Bilotta
bilotta@unina.it

A. Chiaradonna
anna.chiaradonna1@univaq.it

L. Mele
lucia.mele@unina.it

Author's personal copy

L. Pingue
lpingue@trevispa.com

[1] Department of Civil and Environmental Engineering, University of Napoli Federico II, Naples, Italy

[2] Department of Civil, Construction-Architectural and Environmental EngineeringConstruction-Architectural and Environmental Engineering, University of L'Aquila, L'Aquila, Italy

[3] Department of Sustainability Engineering, University Guglielmo Marconi, Rome, Italy

[4] TREVI S.p.A., Cesena, Italy